Received: 2 March 2023 | Revised: 20 April 2023 | Accepted: 22 May 2023

DOI: 10.1002/mawe.202100023

ARTICLE

WILEY VCH

Study on dislocation density, microstructure, and mechanical properties of P92 steel for different heat treatment conditions

Studie über Versetzungsdichte, Gefüge und mechanische Eigenschaften von P92-Stahl bei unterschiedlichen Wärmebehandlungsbedingungen

G. Sharma[1] | **D. K. Dwivedi**[2] | **P. Sharma**[3]

[1]Department of Mechanical Engineering, KIET Group of Institutions, Delhi-NCR, Ghaziabad, Uttar Pradesh, India

[2]Department of Mechanical & Industrial Engineering, Indian Institute of Technology Roorkee, Uttarakhand, India

[3]Department of Mechanical Engineering, ABES Engineering College Ghaziabad, Uttar Pradesh, India

Correspondence
G. Sharma, Department of Mechanical Engineering, KIET Group of Institutions, Delhi-NCR, Ghaziabad, Uttar Pradesh 201206, India.
Email: gaurav.sharma@kiet.edu and gauraviitr1992@gmail.com

Funding information
Ministry of Steel India, Grant/Award Number: 11(1)/SDF/2010-TW

Abstract

The impact of various heat treatment procedures on microstructure, dislocation density, hardness, tensile characteristics, and impact toughness of P92 steel was examined in the current experiment. The martensitic microstructure and average microhardness of 463 HV 0.2 ± 8 HV 0.2 of the normalized steel were prevalent. A tempering procedure was carried out at 760 °C for a range of 2 hours to 6 hours. Additionally, an X-ray diffraction examination was carried out, and the results were used to determine the dislocation density. The normalized sample was characterized by a high dislocation density. The dislocation density was decreased by tempering of normalized samples. With an increase in tempering time, the effect of the treatment coarsened the grains, precipitates, and decreased the area fraction of precipitates. After tempering, MX, $M_{23}C_6$, and M_7C_3 types precipitates were found to have precipitated, according to energy dispersive spectroscopy and x-ray diffraction research. The ideal tempering period was determined to be 4 hours at a tempering temperature of 760 °C based on the microstructure and mechanical characteristics. Steel that was tempered at 760 °C for 4 hours had a yield strength of 472 MPa, an ultimate tensile strength of 668.02 MPa, and an elongation of 26.05 %, respectively.

KEYWORDS
dislocation density, fracture surface, tensile strength, toughness

SCHLÜSSELWÖRTER
Bruchfläche, Festigkeit, Versetzungsdichte, Zähigkeit

TABLE 1 Chemical composition of as received P92 steel.

Elements	C	Mn	Ni	Cr	Mo	Si	P	Nb	V	W	Fe
P92 steel	0.09	0.39	0.18	8.94	0.41	0.11	0.01	0.06	0.18	1.59	Balance

1 | INTRODUCTION

It is imperative to design and produce new heat-resistant steels so that the power plants can run at high temperature and pressure in order to enhance the efficiency of the thermal power plants and safeguard the environment by lowering the emission of carbon dioxide gas [1–4]. Because of their weak resistance to creep and oxidation, standard chromium-molybdenum steels are not favored for such working circumstances. Because of its outstanding physical and mechanical qualities, creep strength enhanced ferritic P92 steel is regarded a viable material for such applications [5]. With a low thermal expansion coefficient, strong oxidation resistance, high thermal conductivity, and outstanding creep strength, P92 steel has excellent mechanical qualities [6, 7]. This class of steel is mainly used for fabrication of components where the operating temperature and pressure are in range of 580 °C to 625 °C and 250 bar to 300 bar, respectively [8, 9]. By increasing the alloying element composition to 1.5% tungsten, 0.005% boron, and lowering the molybdenum level to 0.5%, the P92 steel was created to increase the creep strength of P91 steel, particularly at high temperatures [10–14]. A 30% hike in high temperature strength of P92 steel over P91 due was due to the solid solution strengthening by tungsten, stabilization of martensite lath structure by $M_{23}C_6$ precipitates and inter lath MX type precipitates. The presence/formation of such precipitates depends on temperature and soaking time of normalizing and tempering [15]. In study of the effect of normalizing and tempering parameter on mechanical properties of P92 steel, the tempering time was the most significant factors effecting elongation as compared to normalizing temperature and time [16]. In present study, the effect of tempering time on microstructure and mechanical properties of the P92 steel was investigated. A quantitative measurement of microstructural parameters like size and fraction of precipitates, grain size and dislocation density have been made. Effects of microstructure on tensile properties and impact toughness have been discussed.

2 | EXPERIMENTAL PROCEDURE

The cast and forged, creep strength enhanced ferritic steel of grade P92 was used in this work. The chemical make-up of base metal shoes 8.94% of chromium, Table 1. The specimens had dimensions of 100 mm×25 mm×10 mm when they were cut and machined. The material was hot forged at 950 °C in its original form. The plates were first normalized at 1050 °C for 1 hour, then cooled with air. The normalized samples were then given a tempering treatment at 760 °C for a range of 2 hours to 6 hours, followed by air cooling to room temperature. Slices from each specimen were made according to normal metallographic practice, which involves polishing followed by an etching process using villela reagent solution, for microstructural research and hardness testing. A field emission scanning electron microscope with energy dispersive spectroscopy was used to characterize the specimens′ microstructural characteristics under all the circumstances. The grain size and precipitate size were measured using matlab software using the line cut program in order to investigate the impact of tempering time on metallurgical parameters. Utilizing an x-ray diffractometer with Cuk_{α} radiation and a scan rate of 1° per minute, an investigation of x-ray diffraction was carried out. The peaks with 2θ values ranging from 20° and 120° were recorded and dislocation density was calculated using Williamson-Hall technique. Vickers hardness testing equipment (Omnitech- S. auto) was used to assess each specimen‘s hardness at five separate points while applying a 200 g load and a 10-second dwell period. The ASTM E-8 standard was followed in the preparation of the tensile test specimens for both the raw steel and all heat-treated conditions. A vertical Instron (5982) tensile testing machine with a strain rate of 3.33 10^{-4} s^{-1} was used for the tensile testing. Three specimens were tested in each condition and average value was reported in each condition. Subsize V-notch Charpy impact toughness specimens were created in accordance with ASTM A370-17 in order to inspect the impact toughness′ relationship with

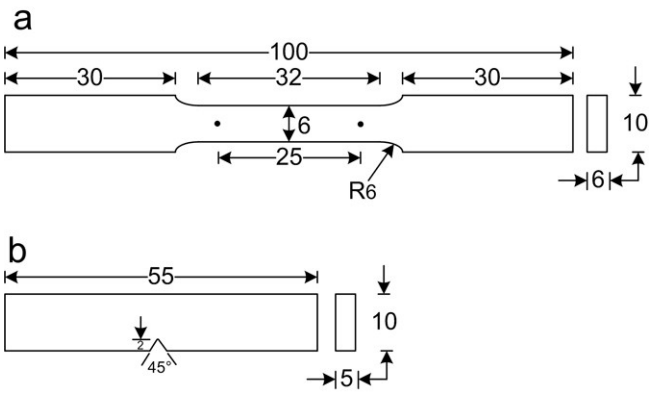

FIGURE 1 Schematic of prepared specimens a) tensile test and b) Charpy impact toughness test.

tempering time, Figure 1. The reduction in area at the fracture point was calculated from the tensile test specimens that had broken. Using a field emission scanning electron microscope, the fracture surface of the tensile and impact specimens was further examined to show the fracture surface topology.

3 | RESULTS AND DISCUSSION

3.1 | Microstructural study

3.1.1 | As received and normalized condition

Cast and forged P92 steel's microstructure in as received state primarily displayed martensitic structure, Figure 2a. Low magnification did not allow for a clear view of the prior austenitic grain boundaries. These boundaries were clearly discernible and represented by dotted lines in the field emission scanning electron microscope picture taken at higher magnification, Figure 2b. Inside these boundaries, martensite laths took the shape of lath packets that were spatially orientated in a single direction. Energy dispersive x-ray spectroscopy investigation was carried out for the interlath area and the prior austenitic grain boundaries, which revealed roughly identical composition throughout the previous austenitic grain boundaries and in the inter lath area due to the precipitates' disintegration, Figure 2c–e. The material was in hot forged condition when it was received, thus to achieve homogeneity in the steel's structure, it was normalized at 1050 °C for 1 hour.

The microstructure of the normalized steel had a lath martensite structure, and it was comparable to the state in which it was received, Figure 3. The martensite laths were orientated in a single direction between the earlier

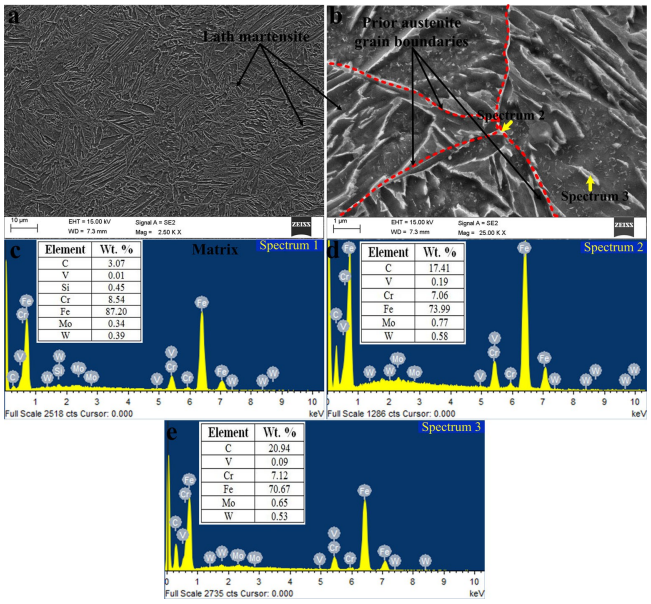

FIGURE 2 Micrographs of the P92 steel in as received condition.

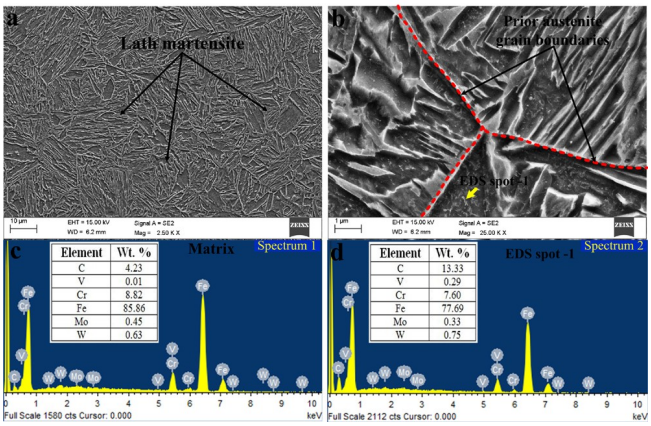

FIGURE 3 Micrographs of the P92 steel in normalized condition.

austenitic grain boundaries. Similar to the spatial orientation seen in the received steel, the lath packets were present in an extended zone. No $M_{23}C_6$ type precipitates was observed after normalizing because during austenization all such precipitates get dissolved. [17]. However, closer observation by scanning electron microscopy revealed few small particles in the inter lath region, Figure 3b. The energy dispersive spectroscopy point analysis suggests that the particles present in the inter lath region were niobium and vanadium rich MX-type, Figure 3d. The austenizing temperature for completely dissolution of the $M_{23}C_6$ and MX type precipitates are 940 °C and 1200 °C, respectively suggesting that all the MX-type precipitates were not completely dissolve during austenizing [18].

3.1.2 | Tempered condition and effect of tempering time

The P92 steel was subjected to air cooling after being held at 760 °C for 2 hours to 6 hours to temper it. The micrographs of steel that has been tempered for two hours had a tempered martensite microstructure with precipitates along the grain boundaries and inter-lath area, Figure 4a–b. Precipitates of the $M_{23}C_6$ type and the MX-type were both found at the prior austenitic grain boundaries and lath boundaries, respectively. Prior austenitic grain boundaries' energy dispersive x-ray spectroscopy study revealed the presence of chromium, molybdenum and tungsten, which suggested $M_{23}C_6$ type precipitates, Figure 4c. It was discovered that the average sizes of the $M_{23}C_6$ and MX type precipitates were 187.27 nm ± 42 nm and 87.94 nm ± 29 nm.

The microstructure of steel that has been tempered for 4 hours and 6 hours was found to be similar to the previous tempered condition, Figure 5a–b. High magnification micrographs were used to quantify the grain size under each tempering circumstance. It was discovered that the grain size grew as the tempering time increased. For 2 h tempering time, the grain size was 20.06 μm ± 7.8 μm which increased to 26.62 μm ± 13.6 μm for 6 hours tempering time, Figure 6. X-ray diffraction analysis also suggests the formation of all these precipitates in various heat-treated condition, Figure 7.

The size and percentage of the precipitates were measured using high magnification micrographs. For the steel that was tempered for two hours, the sizes of the coarse precipitates ($M_{23}C_6$-type) existing at the previous austenitic grain boundaries and the fine precipitates (MX-type) present in the matrix area were 187.2 nm ± 42 nm and 87.9 nm ± 29 nm, respectively. The magnitude of precipitate size increase was extremely considerable for the first 4 hours of tempering and afterwards was comparatively low, indicating that the maximum tempering was accomplished in those 4 hours at 760 °C tempering temperature, Figure 8a. With longer tempering times, the precipitate size likewise grew, reaching sizes of 226.4 nm ± 30 nm and 104.8 nm ± 29 nm after 6 hours. The area fraction of the precipitates was calculated using Image J software, and it was discovered that it decreased with an increase in tempering time, Figure 8b. Grain coarsening was considered to be the cause of the decline in precipitation area fraction over time. Grain coarsening reduces the grain boundary area available for precipitation.

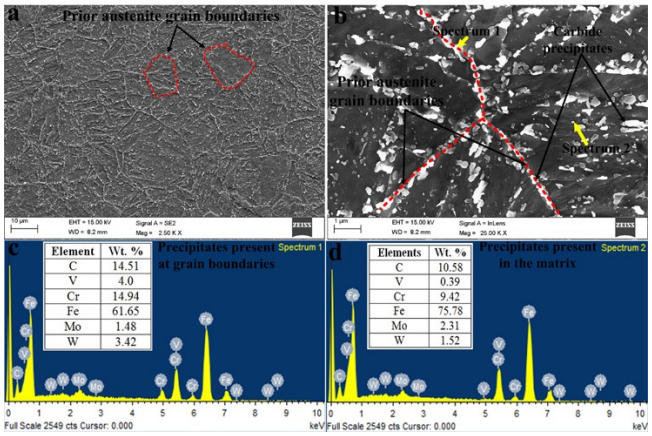

FIGURE 4 Micrographs of the P92 steel in normalized and tempered (1050 °C 1 h /760 °C 2 h) condition.

3.2 | X-ray diffraction line profile analysis

X-ray diffraction pattern for various heat-treated conditions was used for further analysis, Figure 7. Using this

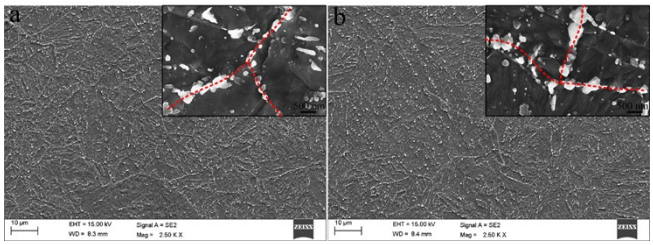

FIGURE 5 Showing scanning electron microscope micrograph in normalized and tempered condition for: a) 4 h and b) 6 h (inset showing the higher magnification view of the precipitates at the grain boundaries).

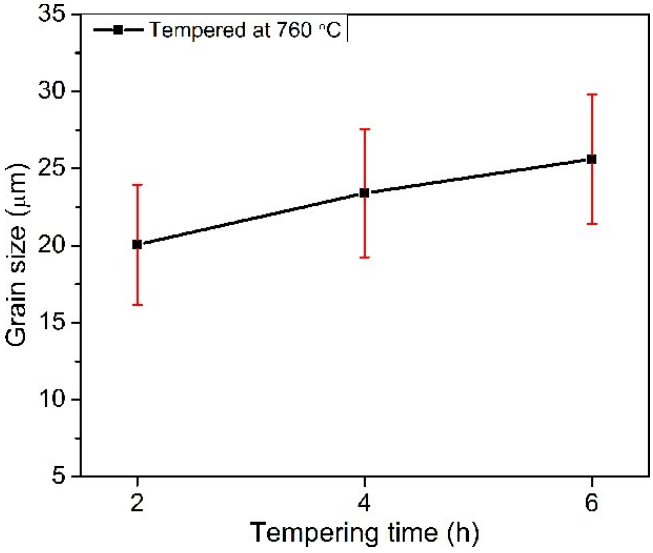

FIGURE 6 Variation of prior austenitic grain size with tempering time.

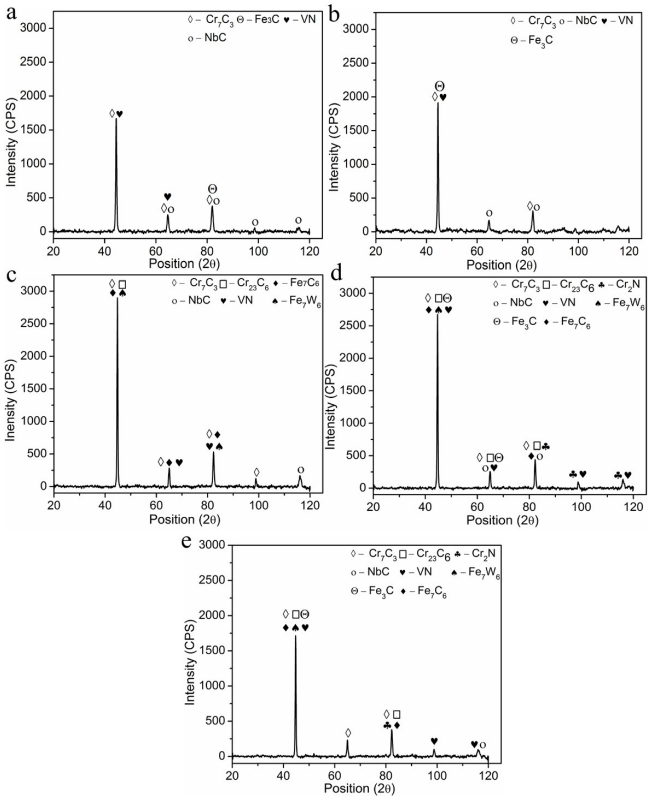

FIGURE 7 X-ray diffraction plots: (a) as received base metal, (b) normalized at 1050 °C, (c) tempered at 760 °C for 2 h, (d) tempered at 760 °C for 4 h and (e) tempered at 760 °C for 6 h.

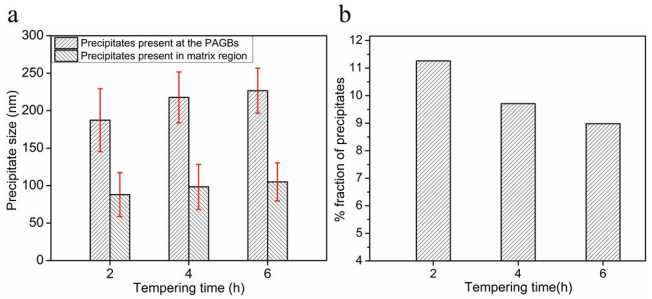

FIGURE 8 Variation of a) precipitate size and b) fraction of precipitate with tempering time.

x-ray diffraction data the peak broadening was calculated for various peaks and the normalized peak intensity plot corresponds to plane (211) were used, Figure 9. Williamson-Hall method was used to calculate the crystallite size and the micro-strain value using Equation 1

$$\beta cos\theta = \frac{0.9\lambda}{D} + 4\ \varepsilon sin\theta \tag{1}$$

where, β is the full width at half maximum (FWHM) for the various peaks. The slope and intercept of the curve

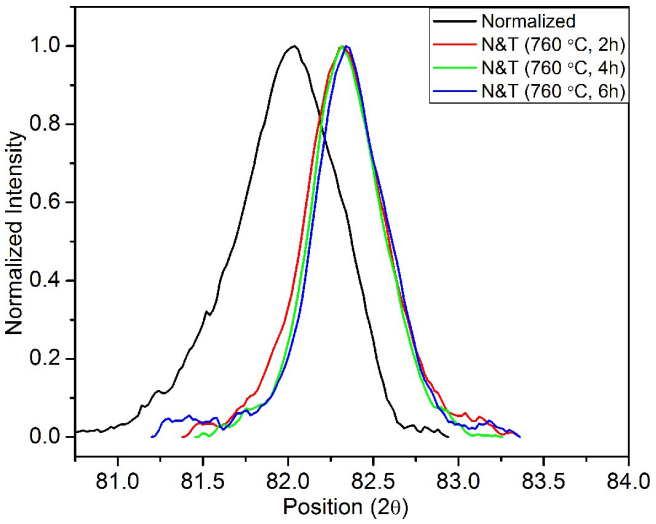

FIGURE 9 X-ray diffraction line profile with normalized peak intensity for P92 steel in various heat treatment conditions.

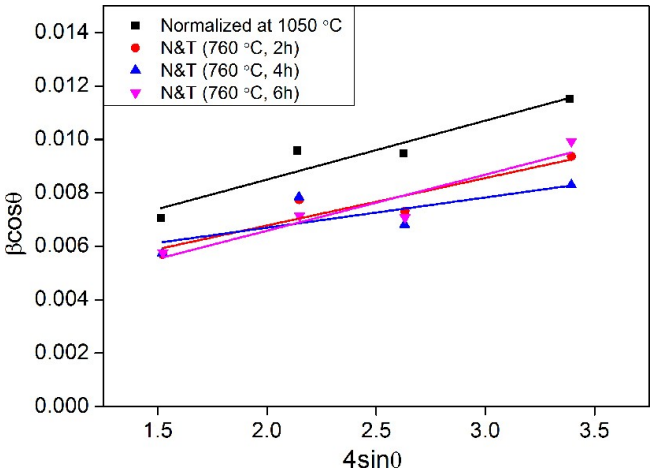

FIGURE 10 Williamson–Hall plot for various heat treatment conditions of P92 steel samples.

βcosθ versus 4sinθ yields the micro strain (ε) and crystallite size (D) values, respectively, Figure 10.

Based on these values, the dislocation density was calculated using the following Equations

$$\rho = (\rho_D \times \rho_s)^{1/2} \tag{2}$$

$$\rho_D = \frac{3}{D^2} \tag{3}$$

$$\rho_s = \frac{k\langle\varepsilon^2\rangle}{b^2} \tag{4}$$

where k = 6π and b is the Burgers vector for body centered cubic iron, and, ρ_D is the dislocation density

TABLE 2 Calculated dislocation density by x-ray diffraction patterns in various heat treatment conditions.

Material state	Heat treatment	Microstructure	Dislocation density ρ [10^{15} m^{-2}]
Normalized	1050 °C, 1 h*	Martensite	1.687
Normalized & tempered	760 °C 2 h**	Tempered martensite	0.977
Normalized & tempered	760 °C 4 h**	Tempered martensite	0.856
Normalized & tempered	760 °C 6 h**	Tempered martensite	0.851

* Followed by air cooling; ** Preceded by normalizing and followed by air cooling

TABLE 3 Tensile properties of the material in various heat treatment conditions.

Material state	Yield strength (MPa)	Tensile strength (MPa)	Elongation (%)	Reduction in area (%)
As received (S −1)	1020.0	1534.20	20.25	50.16
Normalized (S −2)	980.0	1413.77	22.49	58.42
(T 1033 K 2 h AC)	485.0	691.68	23.38	59.22
(T 1033 K 4 h AC)	472.0	668.02	26.05	61.86
(T 1033 K 6 h AC)	467.0	657.09	25.87	66.76

owing to crystallite size and ρ_s is the dislocation density due to strain broadening. After tempering heat treatment, the dislocation density was shown to decrease due to the decomposition of martensite and aggregation of carbide precipitates, Table 2. The tempering period had a negligible impact on dislocation density, though.

3.3 | Mechanical characterization

Micro-hardness, tensile, and V-notch Charpy impact tests were used to describe the mechanical characteristics under various heat treatment conditions. Base metal's hardness in as-received condition was discovered to be 490 HV 0.2±15 HV 0.2, Figure 11. Since the base metal was initially in a hot forged state, as was previously mentioned, a greater hardness was observed due to the untempered lath martensitic microstructure. The hardness in the normalized condition was comparatively lower than the as-received condition having microhardness value of 463 HV 0.2±8 HV 0.2. The untempered martensitic structure and solid solution strengthening of the alloying elements in the matrix owing to dissolution of the precipitates resulting from austenization done at 1050 °C were related with the high hardness. The hardness value saw a dramatic shift after the tempering procedure. The hardness value was seen to decrease with longer tempering times in the tempered condition after normalization. The hardness was 236.9 HV 0.2±6 HV 0.2 for the first two hours of tempering and fell to 220.3 HV 0.2±7 HV 0.2 as the six hour of tempering approached. The rise in precipitate size and area fraction

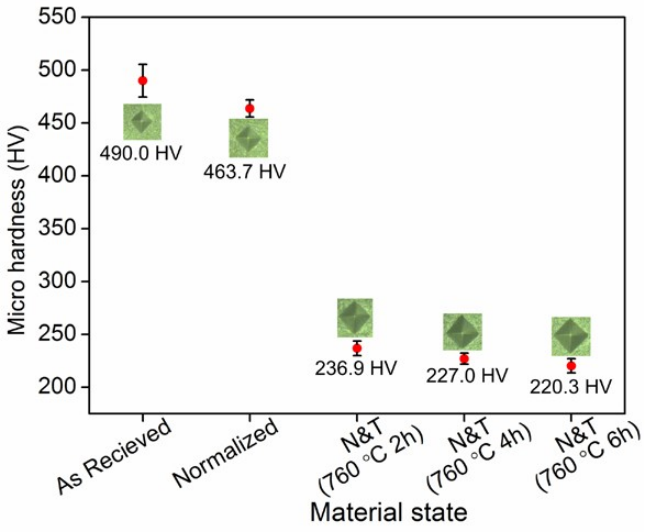

FIGURE 11 Variation in micro-hardness for various heat treatments.

and the decrease in dislocation density with sub-grain formation are responsible for the decrease in hardness with the time of tempering [19].

Base metal and steel were subjected to the room temperature tensile test under all heat treatment conditions. For the as-received condition, the tensile strength, yield strength, elongation, and area reduction were 1534.2 MPa, 1020 MPa, 20.2%, and 50.1%, respectively. Normalized steel has tensile and yield strengths of 1413.7 MPa and 980 MPa, respectively. After tempering, a sizable change in the mechanical characteristics was seen, Table 3. Tensile strength and elongation were

691.6 MPa and 23.3%, respectively, during a 2 hour tempering treatment. The following factors can be used to explain this considerable change: Due to the formation and coarsening of the precipitates, solid solution strengthening elements such as molybdenum and tungsten, among others, diffused into the precipitates during tempering. Additionally, recovery during tempering involved the destruction and rearrangement of dislocations as well as the growth of sub grain structure [20]. As discussed in the previous section, the dislocation density in the normalized condition was 1.687×10^{15} m^{-2} and after tempering treatment, it was reduced to 0.851×10^{15} m^{-2} for 6 hours tempering time, Table 2. Additionally, the tensile and yield strengths fell and the percentage of elongation rose with the length of tempering up to 4 hours, after which only a little change was seen. The maximum tempering can therefore be completed in 4 hours at a tempering temperature of 760 °C. As previously mentioned, extended tempering times coarsen the precipitates, which reduces their capacity to operate as a dislocation barrier, which in turn, causes the material's tensile strength and yield strength to diminish.

Additionally, it was found that as tempering time was extended from 2 hours to 4 hours, the percentages of elongation and decrease in area went from 23.38% and 59.22% to 26.05% and 66.85%, respectively, Figure 12. However, after 4 hours, no discernible change was seen Figure 13. The cracked surface was revealed using field emission scanning electron microscopy examination. In the as received state, fractured surface had a significant number of radial outward-moving fractures known as splitting [21]. Very small dimples were seen in a detailed inspection of the cracked surface in addition to a few micro holes and cleavage facets, Figure 14a, b. Very few tiny fractures were visible at the surface of the tensile test specimen in its normalized state, Figure 14c. When viewed under a microscope, the fractured surface displayed a mixed form of fracture with tear ridges, microcracks, and a minor percentage of dimples, Figure 14d. After tempering, ductile dimples served as the primary distinguishing feature of the shattered surface. It was shown that when tempering time rose, the percentage of dimples also increased, Figure 15b, c.

For all heat treatment settings, the Charpy V-notch impact toughness test was used to quantify impact toughness. The P92 steel has a 34 J and 40.5 J hardness in its as-received and normalized conditions, respectively. Due to the existence of lath martensitic microstructure, the toughness is low under these circumstances. Toughness was determined to be substantially greater (72 J to 77 J) after

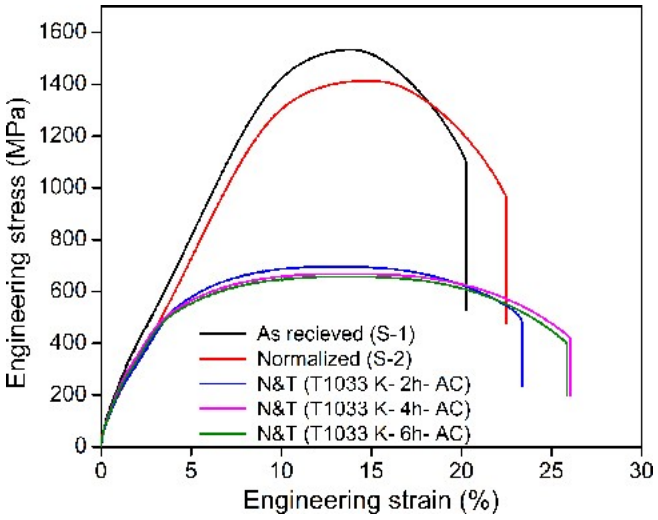

FIGURE 12 Showing Engineering stress vs strain diagram in various heat treatment condition.

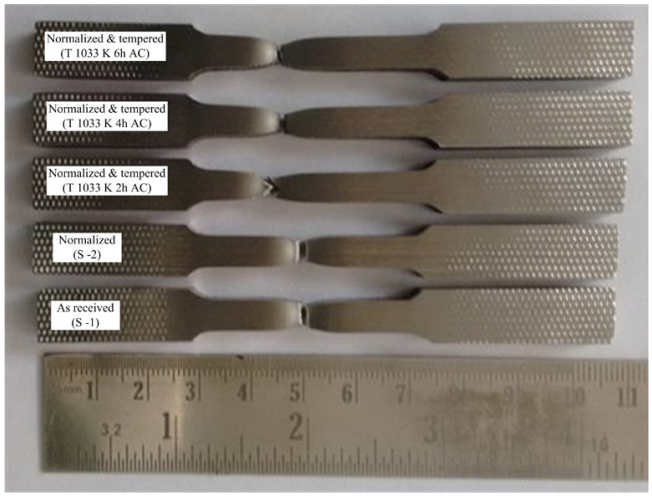

FIGURE 13 Tensile test specimens after testing in various conditions.

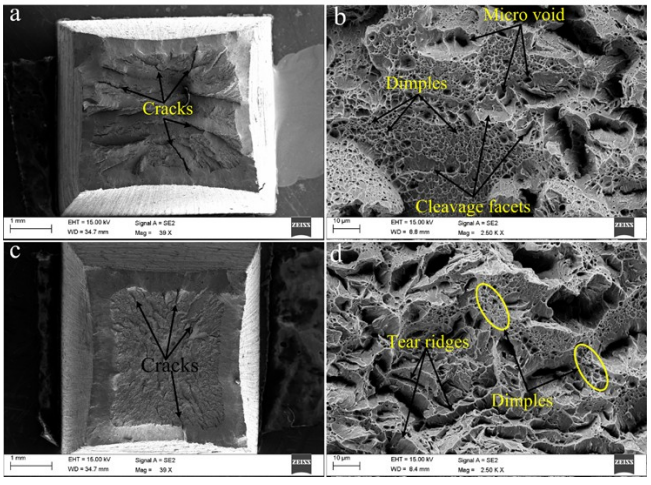

FIGURE 14 Fractured surface morphology of P92 steel after tensile testing for: (a–b) as received base metal and (c–d) normalized at 1050 °C.

TABLE 4 Charpy V-notch impact toughness for as received base metal and different heat treatment condition.

Material state	As received base metal	Normalized (1080 °C, 1 h)	Tempered condition (760 °C)		
			2 h	4 h	6 h
Toughness (J)	34	40.5	72	76	77

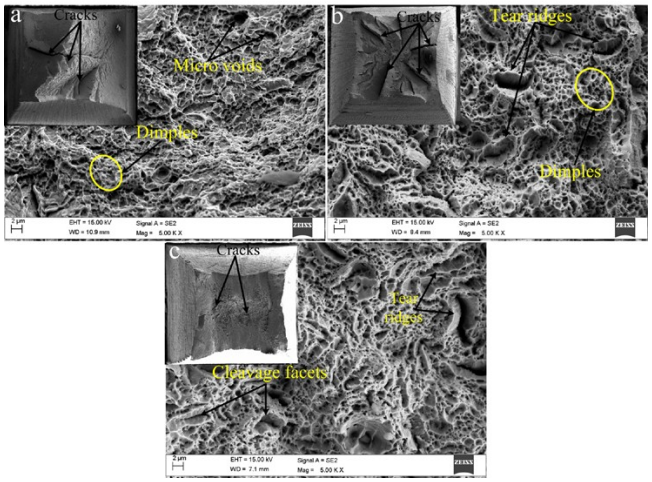

FIGURE 15 Fractured surface for P92 steel after tensile testing for conditions tempered at 760 °C for (a) 2 h, (b) 4 h and (c) 6 h tempering time.

tempering than the as-received condition (34 J). Impact hardness increased from 72 J to 76 J with 2 hours to 6 hours increase in tempering time, Table 4.

Apart from the microcracks and cleavage facets, very few dimples were visible in the material's as-received state, Figure 16a. However, the fraction of dimples was increased after normalization heat treatment, as the tensile test results showed relatively higher reduction in area as compared to as-received condition, Figure 16b. After tempering treatment, the fracture occurred in ductile manner having micro voids and fine dimples at the fractured surface, Figure 16c–e. However, the average dimple size was larger for longer tempering time as compared to the short tempering time.

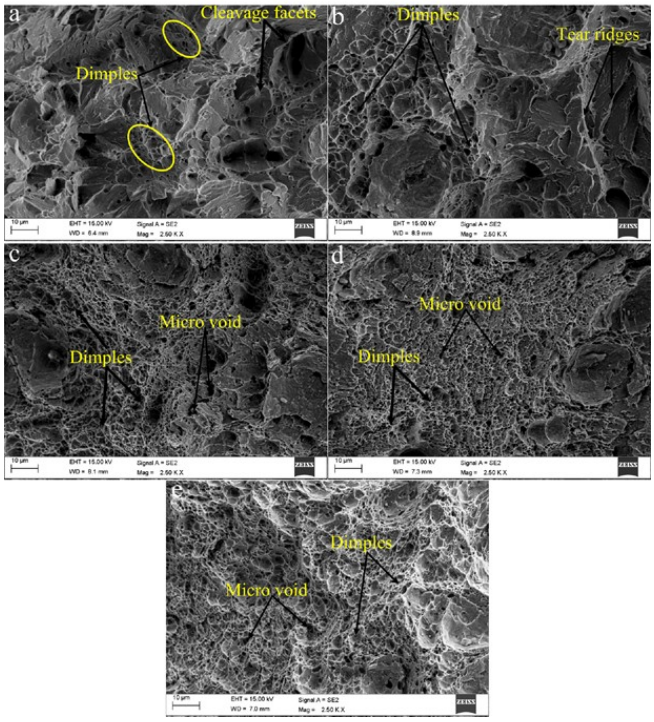

FIGURE 16 Fractured surface for P92 steel after toughness testing for: (a) as received condition, (b) normalized condition, (c) tempered for 2 h, (d) tempered for 4 h and (e) tempered for 6 h.

4 | CONCLUSIONS

In the current investigation, different tempering times were used during the heat treatment of P92 steel. Summarizing the aforementioned research, the following findings may be made:

- P92 steel's precipitation and microstructural stability are affected by tempering time variation, and its yield and tensile strength decrease as tempering time increases.
- According to the mechanical tests of the P92 steel, the ideal tempering may be achieved after 4 hours at a tempering temperature of 760 °C. A tempering period greater than 4 hours has no discernible impact.
- With longer tempering times, the hardness value and strength decreased because to the drop in area fraction and rise in precipitate size.
- In their as-received and normalized conditions, tensile test specimens' shattered surfaces show dimples along with cleavage facets and tear ridges. However, during the tempering procedure, only tiny dimples and micro-voids were seen, and it was discovered that the size of the dimples grew larger as the tempering duration increased.

ACKNOWLEDGEMENT

The authors are grateful the Ministry of Steel India for their financial support for this experimental work under grant no. 11(1)/SDF/2010-TW.

ORCID

G. Sharma http://orcid.org/0000-0003-2837-9377

REFERENCES

1. F. Masuyama, *ISIJ Int.* **2001**, *41*, 612.
2. L. Korcakova, J. Hald, M. A. J. Somers, *Mater. Charact.* **2001**, *47*, 111.
3. W. Xue, P. Qian-gang, R. Yao-yao, S. Wei, Z. Hui-qiang, L. Hong, *Mater. Sci. Eng. A.* **2012**, *552*, 493.
4. D. R. Barbadikar, A. R. Ballal, D. R. Peshwe, J. Ganeshkumar, K. Laha, M. D. Mathew, *Mater. Sci. Eng. A.* **2015**, *624*, 92.
5. G. Sharma, D. K. Dwivedi, *J. Manuf. Process.* **2019**, *38*, 196.
6. T. Sakthivel, K. Laha, P. Parameswaran, S. Panneer Selvi, K. S. Chandravathi, M. D. Mathew, *Trans. Indian Inst. Met.* **2015**, *68*, 411.
7. W. Xue, P. Qian-gang, L. Zhi-jun, Z. Hui-qiang, T. Yong-shun, *Eng. Fail. Anal.* **2011**, *18*, 186.
8. S. H. Babu, G. Amarendra, R. Rajaraman, C. S. Sundar, *J. Phys. Conf. Ser.* **2013**, *443*, 012010.
9. R. Kannan, V. Sankar, R. Sandhya, M. D. Mathew, *Procedia Eng.* **2013**, *55*, 149.
10. K. Sawada, K. Kubo, F. Abe, *Mater. Sci. Eng. A.* **2001**, *319*, 784.
11. K. Maruyama, K. Sawada, J. Koike, *ISIJ Int.* **2001**, *41*, 641.
12. I. Fedorova, A. Kipelova, A. Belyakov, R. Kaibyshev, *Metall. Mater. Trans. A.* **2013**, *44*, 128.
13. P. J. Ennis, A. Z. Lipiec, O. Wachter, A. C. Filemonowicz, *Acta Mater.* **1997**, *45*, 4901.
14. V. Dudko, A. Belyakov, D. Molodov, R. Kaibyshev, *Metall. Mater. Trans. A.* **2013**, *44*, 162.
15. A. Vyrostkova, V. Homolova, J. Pecha, M. Svoboda, *Mater. Sci. Eng. A* **2008**, *480*, 289.
16. S. S. Wang, D. L. Peng, L. Chang, X. D. Hui, *Mater. Des.* **2013**, *50*, 174.
17. C. Hurtado-norena, C.A Danon, M. I. Luppo, P. Bruzzoni, *Procedia Mater. Sci.* **2015**, *8*, 1089.
18. V. Knezevic, A. Schneide, J. Balun, G. Sauthoff, G. Inden, *Mater. Sci. Eng. A.* **2008**, *477*, 334.
19. D. R. Barbadikar, G. S. Deshmukh, L. Maddi, K. Laha, P. Parameswaran, A. R. Ballal, D. R. Peshwe, R. K. Paretkar, M. Nandagopal, M. D. Mathew, *Int. J. Press. Vessel. Pip.* **2015**, *132*, 97.
20. X. Tao, C. Li, L. Han, J. Gu, *J. Mater. Res. Technol.* **2015**, *5*, 45.
21. J. Blach, L. Falat, P. Sevc, *Eng. Fail. Anal.* **2009**, *16*, 1397.

How to cite this article: G. Sharma, D. K. Dwivedi, P. Sharma, *Materialwiss. Werkstofftech.* **2023**, *54*, e202100023. https://doi.org/10.1002/mawe.202100023